Investigation of AHCAL Readout Electronics

Jonas Mikhaeil, University of Heidelberg, Germany

September 5, 2018

Abstract

To increase the jet-energy resolution the particle flow approach was developed. With this method only the most accurate sub-detector measurement is used to determine the energy of each particles in a jet. For this ansatz to work the calorimeter has to be highly granular. This creates new challenges for the readout electronics. In this report the readout electronics for the CALICE AHCAL were investigated. It was shown that modifications to the SiPM coupling of the ASIC to withstand high radiation in the CMS Detector seem applicable under lab conditions. Moreover it was shown that by reducing the length of the bunch clock, a time resolution in the order of 1ns can be achieved. This change is implemented in the ILC Mode.

Contents

1 Introduction

Future collider experiments will require highly granular calorimeters. They allow for an increase of the jet-energy resolution and improved background suppression.

This is especially important for the *international linear collider* (ILC), which is planned to be build in Japan.

As an electron positron collider, the ILC is a precision machine. To increase the jet-energy resolution, the *particle flow approach* was developed. In this method the energy resolution is improved by using the best sub-detector measurements for each particle in the jet.

This requires high granularity to distinguish depositions of charged and neutral particles in the calorimeter.

With these new detectors new challenges for the readout electronics arise. Due to the high channel density the readout electronics are embedded into the active layer of the calorimeter. In this report modifications to the SiPM coupling of the ASICs and the time resolution of the CALICE AHCAL are investigated.

2 The AHCAL

This section will explore the CALICE *Analog Hadronic Calorimeter* (AHCAL). Figure 1 shows the future vision for the AHCAL within the *international large detector*(ILD). The active layers of the AHCAL are segmented into *HCAL Board Units*(HBUs), one of which is shown in figure 1(right). The HBU is equipped with four *application specific integrated circuits* (ASICs). Currently the SPIROC2E is used. Each of these ASICs processes signals from 36 channels. Each channel is equipped with one scintillator tile being read out by one *Silicon Photomultiplier* (SiPM), as shown in figure 2(left). To prevent optical crosstalk, each tile is wrapped in reflecting foil.

A signal produced in a SiPM travels to the ASIC, where it is picked up by a preamplifier. The ASIC then amplifies the signal according to a variable gain. If the initial signal was greater than a variable threshold, a HOLD signal is generated, which leads to the time and amplified amplitude being saved. Instead of auto-triggering by comparing with a threshold, an external trigger can be provided.

The time and amplitude are digitized via a *time to digital-* (TDC) and an *analogue to*
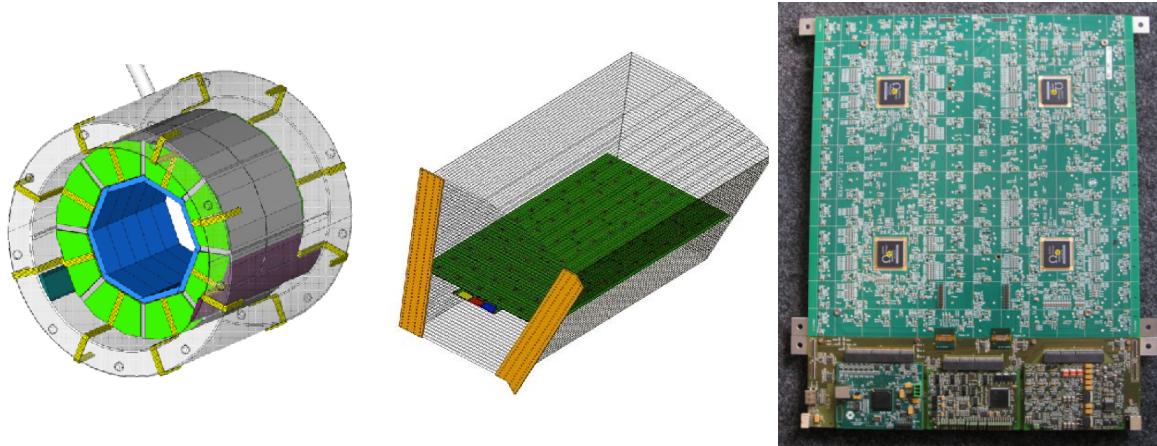
Figure 1: CALICE AHCAL

On the left the concept for the AHCAL barrel. In the middle one barrel sector with one active layer indicated. On the right a single HBU

digital converter (ADC). The TDC consists of a capacitor that samples a voltage ramp (TDC ramp) at the time the signal overcomes the threshold.

The ADC works similar. After an internal delay - the so called *holdtime* - the analog signal is also sampled by a capacitor. Because of the shape of the signal, the holdtime has a considerable effect on the amplitude measured. In Sec.3.1, a new method to estimate the optimal holdtime is developed.

For both ADC and TDC there are 16 of such capacitors, acting as memory cells. In the conversion step, the charge on the capacitors is digitized by the Wilkinson ADC module. More details of the signal path in the SPIROC ASIC can be seen in figure 2

To identify the exact SiPM gain, each channel is calibrated using the integrated LED system.

The LEDs are supplied with a voltage in the order of 5500mV, producing a signal equivalent to a few photons.

The histogram in figure 3 shows the *single pixel spectrum* (SPS) for a typical channel. Due to the photons exciting single pixels in an SiPM, the possible signal amplitudes are quantized. The peaks in the figure correspond to the number of pixel that have fired. The gain is extracted by determining the distance between the first and second peak. This corresponds to the distance between the pedestal and one pixel firing.
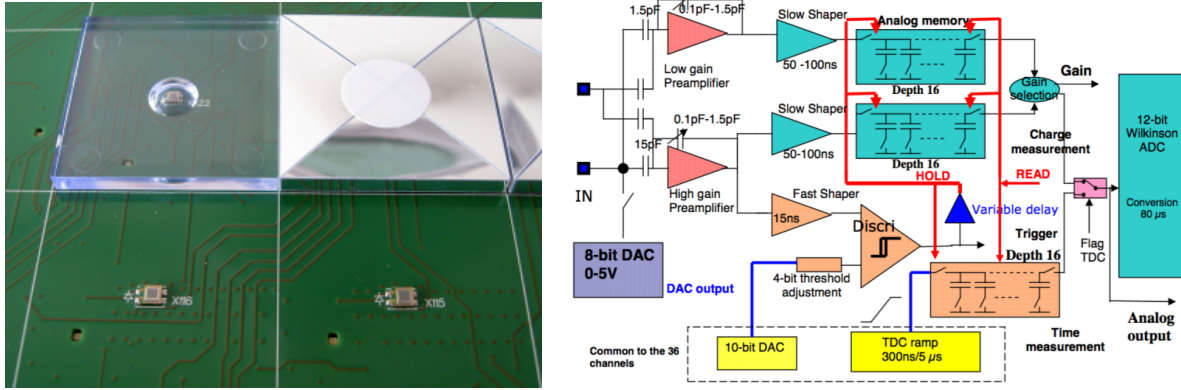
Figure 2: Left: SiPM on the HBU   Right: Schematic of signal path of the SPIROC2[1]
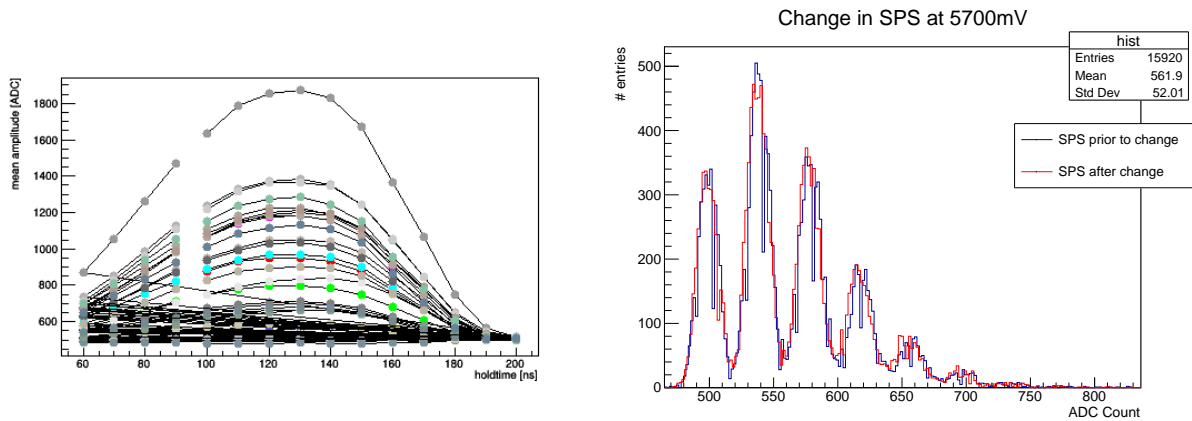

Figure 3: Holdscan: Dependence of the mean amplitude on the holdtime ; Overlap of SPS of one channel before and after the modifications

3 Investigation of changes to the HBU for CMS

For the implementation of the AHCAL in the CMS Detector, the HBU has to be changed. The Radiation induces a large dark current in the SiPM, which leads to a considerable voltage drop over resistances in series with it. In the following the effects of those changes are analyzed.

3.1 Preparation

Firstly the optimal holdtime for the HBU has to be determined. For that a holdscan, varying the holdtime, is performed.

Figure 3 shows the dependence of the mean amplitude on the holdtime. To estimate

the optimal holdtime, one can assume the peaks of the holdcurves to be Gaussian. With this assumption, one can maximize the total output of all channels on a numerical grid.

$$t_{hold} = \max_{t \in G} \sum_{ch}^{\text{all channels}} P_{ch} \exp \frac{(t - \mu_{ch})^2}{\sigma_{ch}^2} \tag{1}$$

Here G is the numerical Grid, P_{ch} the height of the Peak of each channel and μ_{ch}, σ_{ch} are the position and width of the Gaussian, respectively.

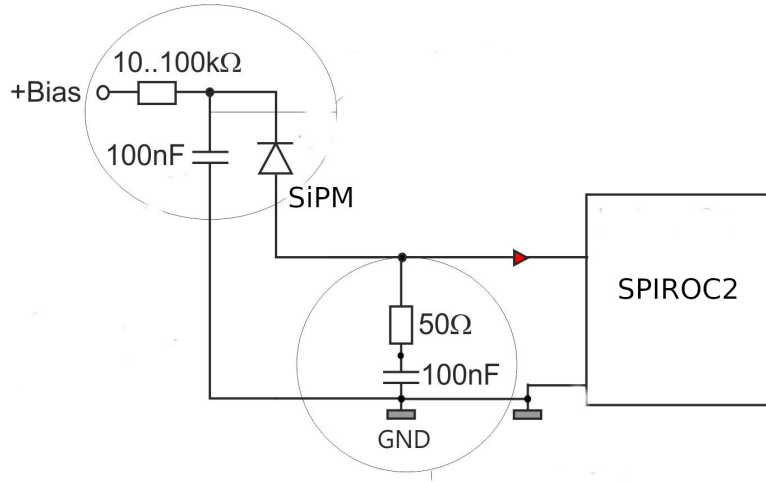Four channels with roughly the same amplitudes at the peak of the holdcurve were chosen.

Figure 4: Schematic of channel setup. Resistance and capacitor in the upper left were removed for multiple channels.

In those a 100kΩ resistor, which is in series with the SiPM, as well as a 100nF capacitor, were removed. An increase in noise - due to the high voltage not being filtered any more - is to be expected. For a crosstalk study, the LED in two other channels was removed as well.

3.2 Investigation of the Effects

In the following, the influence of the implemented modifications of the HBU are being analyzed.

3.2.1 Changes in Gain/Signal to Noise

No apparent change in the SPS in figure 3 before and after the changes is visible. To extract the gain and signal to noise ratio, the SPS is fitted with multiple Gaussians. The width of the first peak is used to estimate the noise. The results from this, see Table.1,

Channel	Gain		Signal to Noise	
	prior	after	prior	after
20	40.15 ± 0.09	39.56 ± 0.08	5.27 ± 0.11	5.3 ± 0.12
24	39.86 ± 0.09	39.06 ± 0.08	5.4 ± 0.13	5.3 ± 0.13
29	40.48 ± 0.09	40.50 ± 0.08	5.7 ± 0.13	5.9 ± 0.13
35	40.54± 0.09	40.39 ± 0.09	5.2 ± 0.12	5.1 ± 0.13

Table 1: Gain and signal to noise before and after modifications to the channels

show no significant change in gain or in the signal to noise ratio.

3.2.2 Optical Crosstalk and Pedestal Shift

While investigating the changes in gain, a non-pedestal signal in a channel without an LED was found.
This hinted at optical cross talk. To quantify that effect, further LEDs were removed, such that the channel had only one neighbouring cell with an LED.
Figure 5 shows the optical cross talk of two channels to be smaller than 1%.
 Moreover *Pedestal Shift* was investigated. This is a known effect which shifts the global pedestal position depending on the total charge injected into the SPIROC Chip.[2] To quantify this, all preamplifiers except for one were turned off. Figure 6 shows the pedestal shift to be increased for the altered channel. Figure 5(right) shows the pedestal position of one modified channel for different board configurations. The measurements colored in red were taken with one preamplifier turned on, the blue ones with all preamplifiers turned off. This indicates a new unknown effect that does not vanish, when no charge is injected into the SPIROC. Further investigation is required.

3.2.3 Auto-Trigger Noise Measurement

Instead of providing an external trigger, the ASIC can also auto-trigger itself.The noise rate was analyzed, to see whether the changes to the board have an influence. In
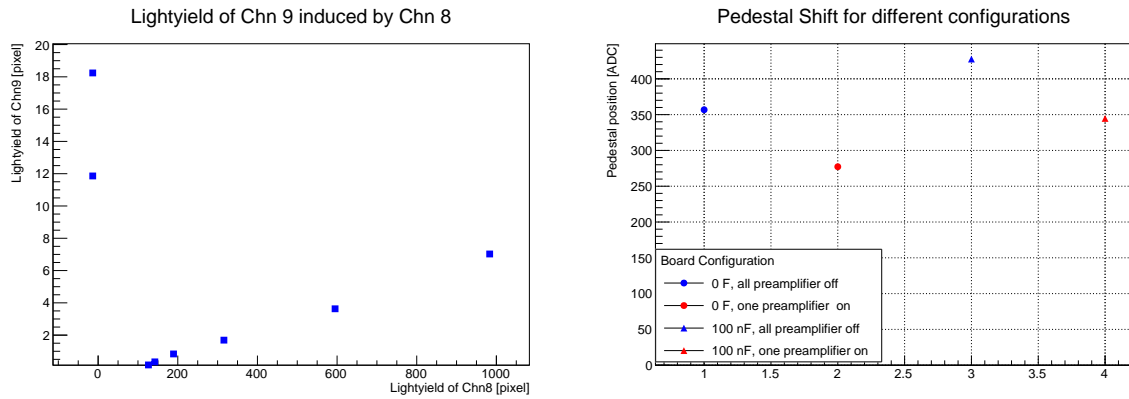
Figure 5: On the left optical crosstalk. Both axis show the lightyield of the corresponding channel. Lightyield is the signal amplitude corrected by the pedestal and divided by the gain. For too large signals the ASIC gives back 0. On the right a Pedestal Shift-like effect. The y-axis shows the pedestal position. Along the x-axis different board configurations.
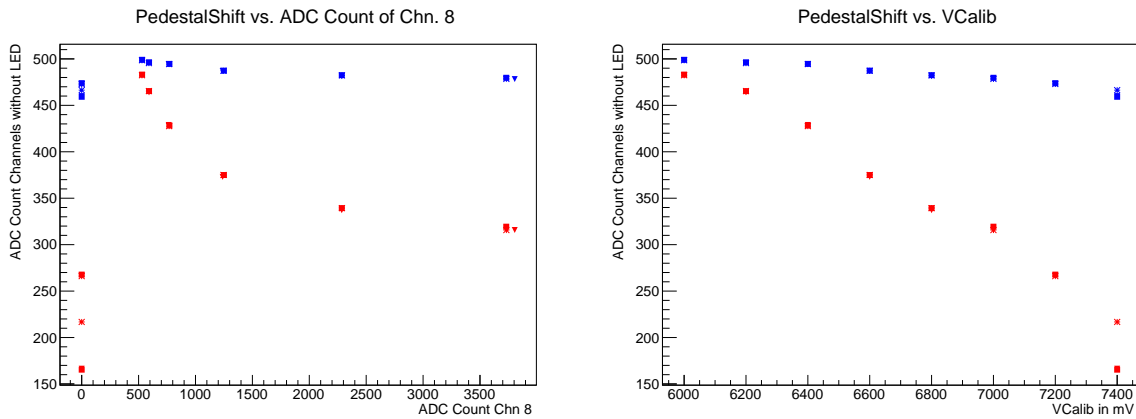

Figure 6: Observed Pedestal Shift. On the left dependence of the Pedestal Shift on the amplitude measured in the only channel with turned on preamplifier. On the right dependence of the Pedestal Shift on the calibration voltage for the LEDs. Different marker styles represent different number of triggers. The upper curve show the effect for a non-modified channel. The lower curves for a channel with both resistor and capacitance removed.
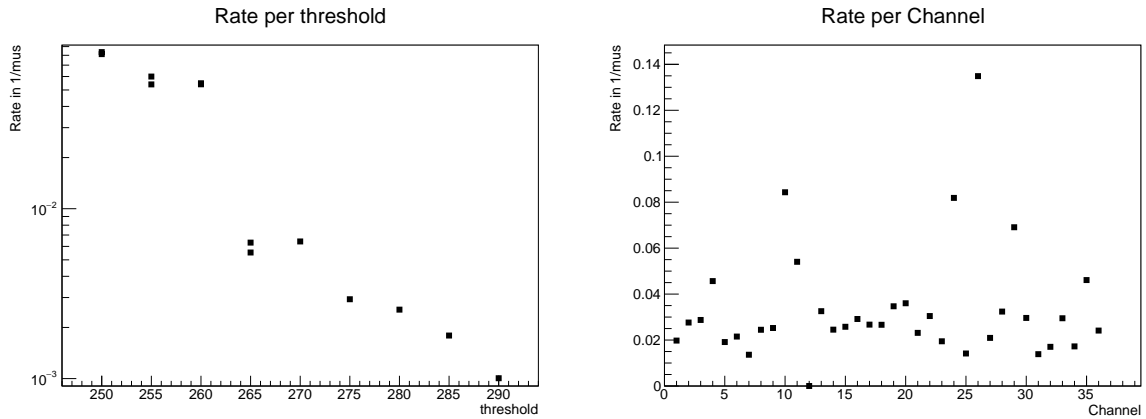
Figure 7: On the left the noise rate in $1/\mu s$ is plotted against the threshold value. The y-axis is logarithmic. On the right the overall noise rate for all channels averaged over all threshold measurements.

figure 7(left) the dependence of the noise rate on the trigger threshold is shown. With increasing threshold, the noise decreases exponentially.

In figure 7(right) no significant effect of our modifications on the noise rate is visible.

3.3 Conclusion

The modifications to the SiPM coupling of the ASIC seem applicable under lab conditions and could help make the CALICE AHCAL suitable for use in the CMS Detector. Further investigation of the Pedestal Shift will be necessary to determine the origin of this effect. Possible sources are the LED system or unknown effects on the ASIC. Moreover the influence of an irradiated SiPM on our modifications should be tested.

4 Investigation of the AHCAL Time Resolution

To improve the reconstruction of hadronic showers in the AHCAL, time information could be used. For that an improvement in time resolution is necessary. In this section we want to analyze the ILC Mode for the SPIROC2, which shortens the Bunch clock from $4\mu s$ to $200ns$ - increasing the slope of the TDC ramp by a factor of 20. In theory this should improve the time resolution from roughly 5ns, measured in Testbeam Mode[1], to about $5ns/20 = 250ps$.

In the following section the TDC ramp for both the ILC Mode and Testbeam Mode will
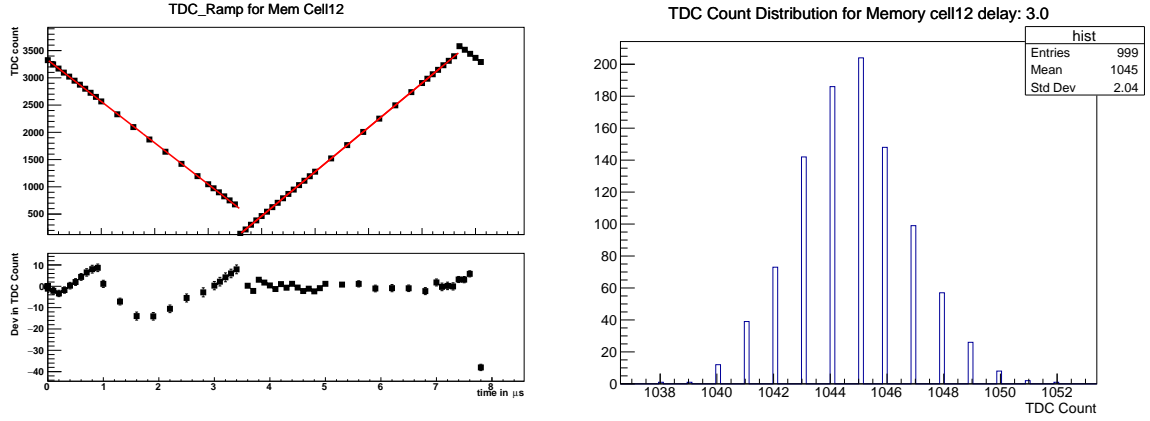
Figure 8: TDC Ramp and TDC Count Distribution for one Delay Time in Testbeam Mode.

be investigated. In the end the time resolution of the ILC Mode will be determined with cosmic muons. This is done by measuring their speed, which is expected to be very close to the speed of light.

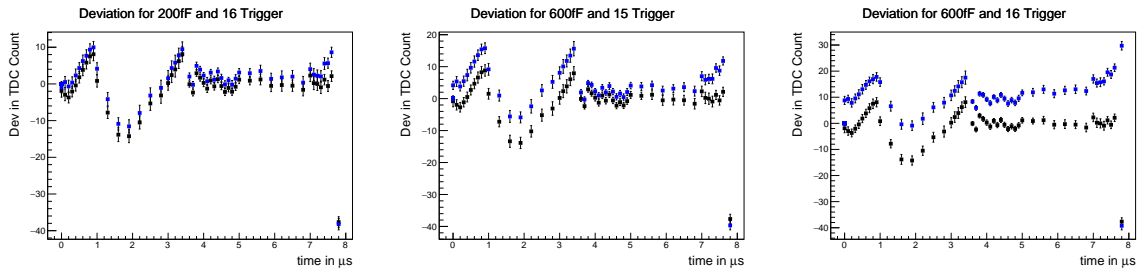## 4.1 Analysis of the TDC Ramp with a Pulse Generator

Figure 9: Deviation between TDC Ramps for different number of triggers and different gain. The black reference values are from 200fF amplification and 15 triggers.

A pulse generator allows to inject a well timed signal of known amplitude into one of the channels of the HBU. This makes a high precision scan of the TDC ramp possible by providing an external trigger and injecting the pulse after a variable delay.

Figure 8 shows the TDC ramp for one memory cell of one channel in Testbeam mode. The ramp is not entirely linear with deviations from linearity being in the order of 10 TDC counts.

The measurement was repeated with different amplification and increased number of
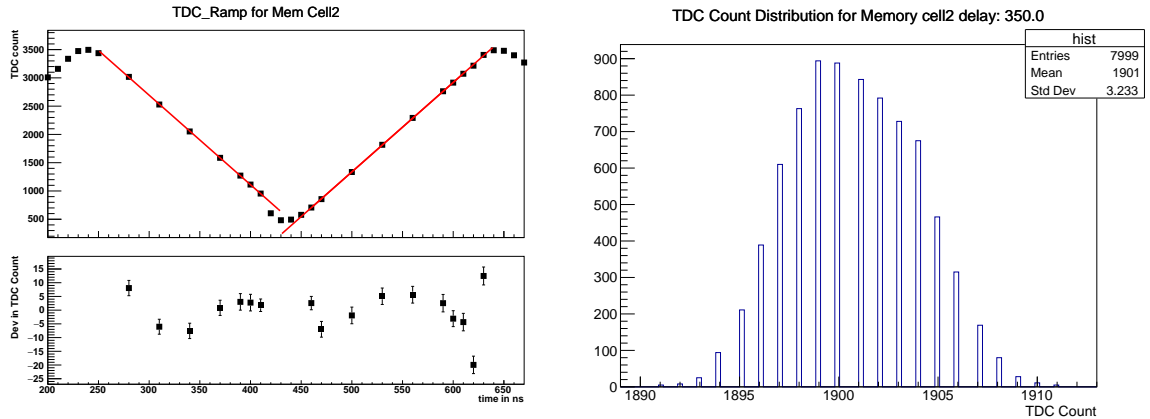
Figure 10: TDC Ramp and TDC Count Distribution for one Delay Time in ILC Mode

triggers. To see whether these changes have an effect on the TDC ramp, the observed ramps were fitted with the slope obtained above. Figure 9 shows that both the amplification and the number of triggers have an influence on the ramp.

The analysis of the TDC ramp in ILC mode, see figure 10, shows the linearity at the edges of the bunch clock to be worse than in Testbeam mode. This is due to the multiplexer between ramps being too slow and the slope of the ramp not yet being optimized for ILC mode. In the middle of the falling and rising part, the deviation is roughly the same as before.

The purely electronic time resolution - without effects originating in the scintillator or the SiPM - can be estimated by converting the width of the TDC count distribution with the fitted slope of the TDC ramp. This yields $\Delta t_{elec,Testbeam} = 2.7ns$ as the electronic time resolution for the Testbeam mode and $\Delta t_{elec,ILC} = 204.3ps$ for the ILC mode.

4.2 Analysis of the Time Resolution in ILC Mode

To investigate the time resolution of the ILC mode, the speed of light was measured. To do so, the setup was moved 12 meter underground to HERA Hall West capturing signals from cosmic muons.

4.2.1 Setup

The setup consists of two scintillator plates and two HBUs.
The scintillators are used for validation. This way only events, that produce a signal in both scintillators are analyzed, distinguishing between muons and noise. The distance
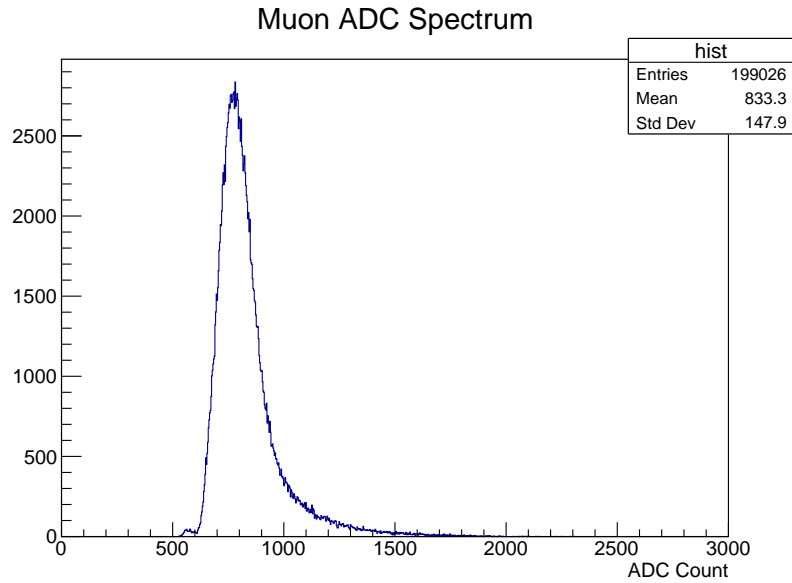
11

Figure 11: Spectrum of the energy deposition in one HBU of a muon. This is a well known MIP spectrum.

measured between the HBUs is $38.8 \pm 0.1cm$.

With this length scale a time resolution in the order of 1ns will be necessary to determine the speed of a muon.

4.2.2 It's a Muon

Muons are minimal ionizing particles (MIPs). These are used to calibrate the energy scale of the AHCAL. The spectrum of their energy deposition is thus well known.

In figure 11 we see the energy deposition spectrum for one of our HBUs in the cosmic teststand. It resembles the expected curve for MIPs - a Landau distribution convoluted with a Gaussian - nicely. Being underground, we can be sure that this signal is created by muons.

4.2.3 Calibration of the TDC Ramp

To be able to measure the time of an event, the TDC ramp has first to be calibrated with a time reference. The time reference is given by the *Beam Interface* (BIF).[1] Each BIF tick is equivalent to 0.78125ns

---

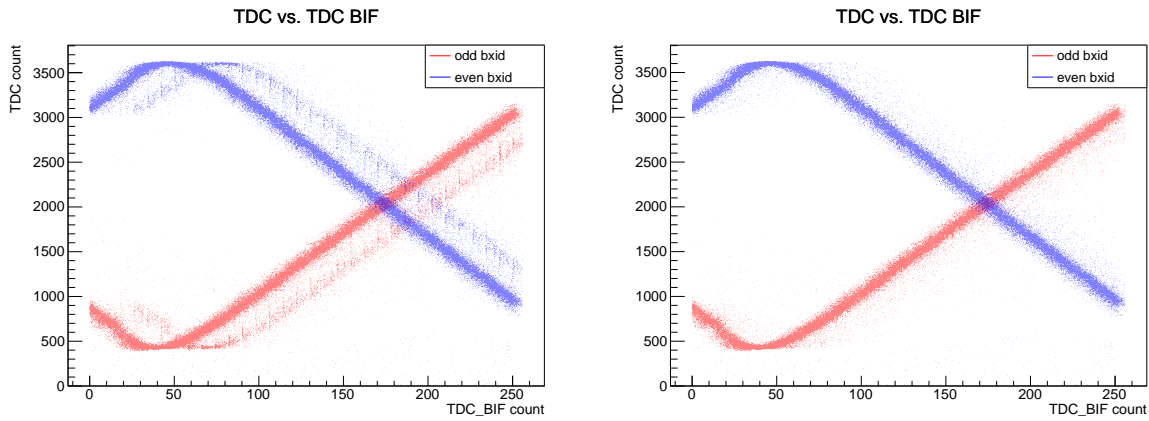[1]For more information about the BIF, see [3]

12

Figure 12: TDC Ramp in reference to BIF time for odd and even Bunch Crossing IDs. Second Figure is corrected for after trigger effects
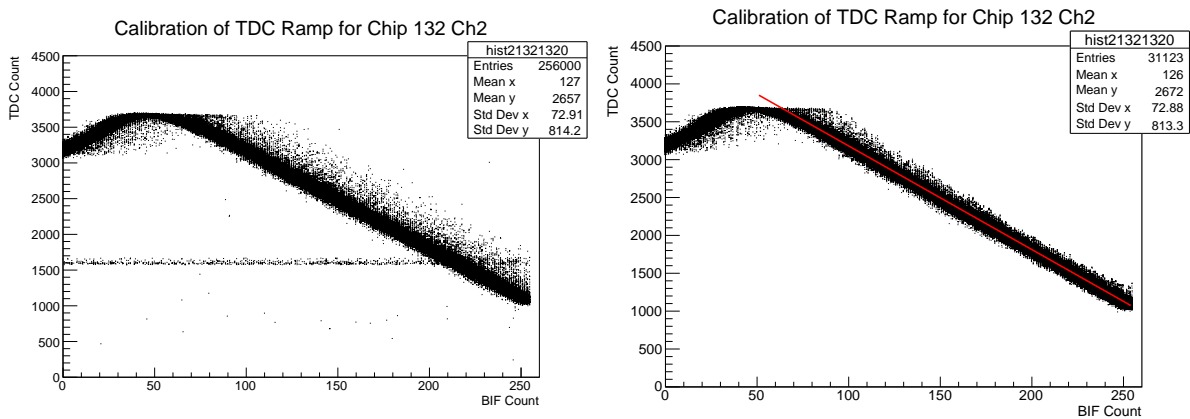

Figure 13: Calibration of TDC ramp for single chip, channel and Bunch Crossing ID. On the right noise is cut away and a linear fit is applied.

Figure 12 shows the TDC ramp for odd and even Bunch Crossing IDs relative to the time given by the BIF.

In the left figure a second ramp shifted along the BIF axis is clearly visible. This is seems to be an effect due to one trigger triggering more than once. This should be investigated further.

It was corrected by not accepting any new trigger within 50ns after the previous one.

Due to small differences between channels, the TDC ramp has to be calibrated for each of them separately.

Figure 13(left) shows that the TDC ramp for a single channel is still quite noisy. To
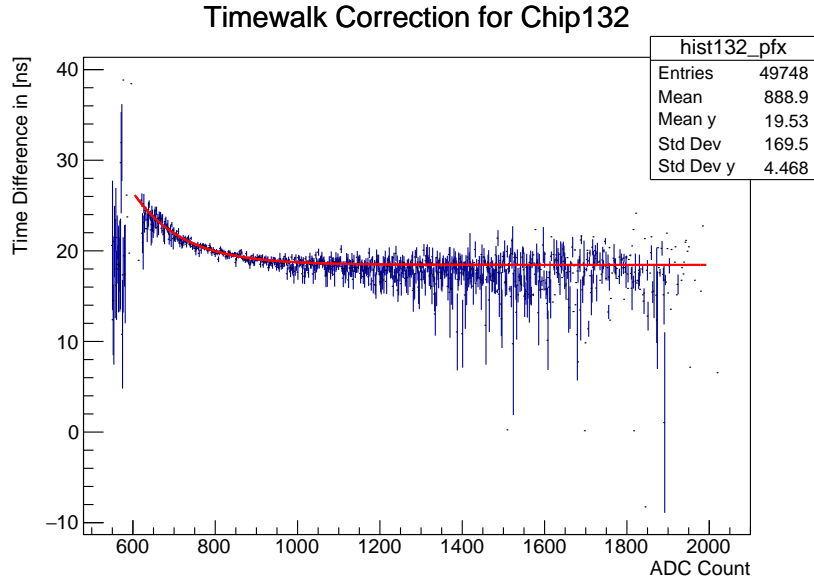
Figure 14: Time Walk Effect for one chip. The measured TDC value depends on the amplitude of the signal. Small amplitude signals trigger systematically too late.

increase the calibration quality, the noise is cut away as seen in the right figure. This was done by applying a cut to each BIF bin, removing all TDC values straying more than two standard deviations from the mean. A linear fit is then applied to convert TDC values to BIF time.

4.2.4 Correcting for Time Walk

Due to an amplitude threshold in the TDC readout, signals with small amplitudes will systematically trigger later than high amplitude signals. This leads to a time shift depending on signal strength. This effect is called *Time Walk*.

A correction can be obtained by plotting the difference between the reference time (BIF time) and the TDC time against the signal strength (ADC count).[1] A chip wise correction seemed necessary. Figure 14 shows the Time Walk effect for one chip.

A fit of the form $a\, e^{bx+c} + d$ describes the data well.

4.2.5 Measuring the Speed of Muons

With the TDC ramp being calibrated, the travel time of the muons can be extracted.

Having calibrated both HBUs separately, the distribution of the time difference for each muon event should be symmetrically centered around 0ns. Figure 15 shows that
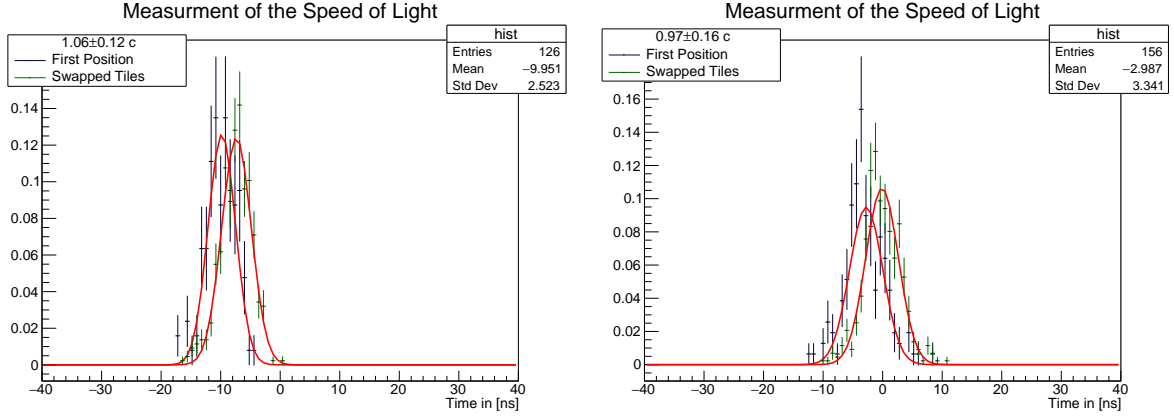
14

Figure 15: Time Difference of muon events for both HBU positions.
Even Bunch Crossing IDs on the left, odd ones on the right

this is not the case. The offset of the histogram is different for odd and even Bunch Crossing IDs. This is probably due to not correcting for the TDC pedestals in the TDC calibration. Both Bunch Crossing IDs have to be treated separately.

Switching the position of the HBUs leaving the calibration unchanged, produces a shift in the peak position of the histogram corresponding to the time it took the muon to travel twice the distance between the HBUs.

To reduce the uncertainty of the distance traveled by the muon, only events that where detected in channels directly on top of each other, where analyzed.

The speed of the muons can now be calculated by dividing the distance of the HBUs by the time extracted from figure 15. Combining our results for odd and even Bunch Crossing IDs,

$$c_{muon} = 1.015 \pm 0.10c$$

is obtained. This result is consistent with the expected velocity for cosmic muons - the speed of light.

4.3 Conclusion

Using a pulse generator we could show that the TDC ramp in ILC mode has a linear shape with deviations from linearity comparable with the Testbeam mode.

In our measurement with cosmic muons, we were able to measure the speed of light with an uncertainty of 10%.

By extracting the width of the Gaussian fit in figure 15, the time resolution can be

estimated. The histogram shows the difference of the time measurement of both HBUs. Assuming the contribution of both channels to be the same, the time resolution is given by

$$\Delta t = \frac{\sqrt{\sigma_{\text{HBU 1}} + \sigma_{\text{HBU 2}}}}{2} \approx \frac{\sigma_{Gaus}}{\sqrt{2}}$$
$$= 1.76ns$$

This is an improvement by a factor of three compared to the time resolution of 5.2ns in Testbeam mode . This comparison has to be judged with care, due to the fact that the time resolution for the ILC mode was obtained in a different way than for the Testbeam mode.[1] Further analysis of the ILC mode at a Testbeam and improvement of the calibration process, e.g. correction for non-linearity and TDC pedestal correction, will be needed to get a more accurate estimation of the time resolution of the ILC Mode.

References

[1] Time development of hadronic showers in a Highly Granular Analog Hadron Calorimeter, pp. 111-112 *E. Brianne*

[2] Commissioning and LED System Tests of the Engineering Prototype of the Analog Hadronic Calorimeter of the CALICE Collaboration, pp. 96 *O. Hartbrich*

[3] https://www.ohwr.org/projects/fmc-mtlu/wiki/aida-mini-tlu